Journal of Power Sources 194 (2009) 931–940

Contents lists available at ScienceDirect

Journal of Power Sources

journal homepage: www.elsevier.com/locate/jpowsour

Analysis and optimization of flow distribution in parallel-channel configurations for proton exchange membrane fuel cells

Weigang Zhang, Peng Hu, Xinmin Lai*, Linfa Peng

State Key Laboratory of Mechanical System and Vibration, Shanghai Jiao Tong University, Shanghai 200240, China

ARTICLE INFO

Article history:
Received 30 March 2009
Received in revised form 15 May 2009
Accepted 18 May 2009
Available online 23 May 2009

Keywords:
Parallel channels
Flow distribution
Optimization
Linear analytical model

ABSTRACT

Parallel channels have many advantages, such as low pressure drop and easy fabrication, but they may cause flow maldistribution which would result in low reaction efficiency. This study presents an analytical model to calculate the flow distribution of the parallel channels based on the assumption of the analogy between fluid flow and electrical network. The model, which ultimately releases from the solution of a set of nonlinear equations, is validated by comparing with the results obtained from three-dimensional computational fluid dynamics (CFD) simulations. Consequently, the model is used to optimize the geometric dimension of a parallel plate to obtain a uniform flow field distribution.

1. Introduction

Proton exchange membrane fuel cells (PEMFC) are considered to be advanced power sources for their high efficiency and low pollution. Bipolar plates are important components of the PEMFC, which help to distribute the reactant gas, collect current, provide structure support, facilitate water and heat management [1]. Many designs of flow configurations, for example, serpentine, parallel discontinuous [2] and interdigitated channel (Fig. 1), are currently used. There are two principal considerations in the choice of a particular configuration: (i) the overall pressure drop; (ii) the degree of non-uniformity of flow distribution over the plate [3]. Serpentine channels have good flow distribution but may have high pressure drop, while parallel channels have low pressure drop but may cause flow maldistribution which would result in severe problems. For example, some channels may be staved of reactants, while others may have excessive reactants.

Generally, there are two kinds of method calculating the flow distribution of bipolar plates: (i) CFD simulation and (ii) analytical method. With the development of computer technology, CFD simulations are usually more accurate than analytical models, but they always cost more time and money. As a result, it is hard to optimize the geometric parameters of the bipolar plates to fix the flow maldistribution of parallel channels using CFD simulations due to numerous calculations.

Some researches, dealing with the flow maldistribution of the parallel channels, have been reported. Ma et al. [4] considered the consequences of a non-uniform gas distribution using a computational model. Pei [5] studied the hydrogen pressure characteristics. Kee et al. [6] raised the possibility of maldistribution and presented a numerical model to calculate the flow distribution in a Z-type parallel configuration. Maharudrayya et al. [7] analyzed U-type parallel configurations and obtained closed form analytical solutions to calculate the flow distribution and the pressure drop in simple parallel channels. Jung et al. [8] developed a 2-D model to analyze the flow and pressure distributions. Shimpalee et al. [9] numerically investigated how serpentine flow-fields with different channel/rib's cross-section areas affect performance and species distributions for both automotive and stationary conditions. Furthermore, Koh et al. [10] presented a resistance concept based model for to evaluate the flow distribution among cells in a fuel cell stack. Ma [11] and Karimi [12] used network flow analysis to calculate flow distribution within fuel cells with nonlinear methods. However, a simple design procedure that can be used for the optimization of the parallel flow field is not available.

Against this background, the present work proposes a simple linear computational model for the purpose of optimization design to resolve the problem of maldistribution. Three-dimensional CFD simulations are also performed to validate the model and optimization results.

2. Theory

2.1. Assumptions

The model is set up based on the following assumptions:

* Corresponding author. Tel.: +86 021 34206303; fax: +86 021 62932125 103.
E-mail addresses: wgzhang@sjtu.edu.cn (W. Zhang), hup@sjtu.edu.cn (P. Hu), xmlai@sjtu.edu.cn (X. Lai), penglinfa@sjtu.edu.cn (L. Peng).

0378-7753/$ – see front matter © 2009 Elsevier B.V. All rights reserved.
doi:10.1016/j.jpowsour.2009.05.033

Nomenclature

A_c	cross-sectional area of channel (mm^2)
A_h	cross-sectional area of header (mm^2)
A_i	cross-sectional area of the ith channel (mm^2)
b_c	depth of channel (mm)
D_c	hydraulic diameter of channel (mm)
f	friction factor
F	non-uniformity index
L_c	length of channel (mm)
$l(i)$	width of channel (mm)
$L(i)$	length of the header between each channel (mm)
n	number of channels
p_{in}	pressure at inlet (Pa)
p_{out}	pressure at outlet (Pa)
P_c	cross-sectional perimeter of channel, mm
r_i	resistance of the ith channel
R	resistance
R_i	resistance of the inlet header between ith and $i+1$th channel
$R_{i'}$	resistance of the outlet header between ith and $i+1$th channel
R_L	resistance of the center of L shape corner
R_T	resistance of the center of T shape corner
Re	Reynolds number
$\bar{v}$	mean velocity ($mm\,s^{-1}$)
v_i	mean velocity in the ith channel ($mm\,s^{-1}$)
V_i	mean velocity in the inlet header between ith and $i+1$th channel ($mm\,s^{-1}$)
$V_{i'}$	mean velocity in the outlet header between ith and $i+1$th channel ($mm\,s^{-1}$)
V_{in}	inlet velocity of the plate ($mm\,s^{-1}$)
w_c	width of channel (mm)

Greek letters

α	channel aspect ratio (width/depth)
μ	viscosity
ρ	mass density
τ_w	wall shear stress

1. The analysis here assumes the flow properties (e.g. the mass density, the viscosity) are constant.
2. The Reynolds numbers are low, the flow is considered as laminar flow and the temperature is nearly uniform.
3. The reactant gas is considered to flow in impervious channels. It does not consider the mass flow between the reactant channel and electrolyte. It is a significant assumption which is necessary for simplifying the model [13].

2.2. Hagen–Poiseuille flow

For a straight channel, steady Hagen–Poiseuille flow, pressure drop is needed to balance shear stress caused by the walls.

$$(p_{in} - p_{out})A_c = \tau_w P_c L_c \tag{1}$$

where p_{in} and p_{out} are the pressure of the inlet and outlet of the channel, respectively. A_c is the channel cross-sectional area. P_c is the channel cross-sectional perimeter, and L_c is the channel length.

The shear stress can be represented by using the friction factor f as follows:

$$f = \frac{\tau_w}{1/2\rho\bar{v}^2} \tag{2}$$

where $\bar{v}$ is the mean velocity of the channel. Here, f is the friction factor given by the empirical correlation of Kays and Crawford [14]

$$\mathrm{Re}\, f = 13.84 + 10.38 \exp\left(\frac{-3.4}{\alpha}\right) \tag{3}$$

where $\alpha = w_c/b_c$ is the channel aspect ratio.and the Reynolds number is

$$Re = \frac{\rho\bar{v}D_c}{\mu} \tag{4}$$

where D_c is the hydraulic diameter $D_c = 4w_c b_c/2(w_c + b_c)$.

From Eqs. (1)–(4), we get

$$\Delta p = p_{in} - p_{out} = \frac{1}{2}\frac{(\mathrm{Re}\, f)\mu P_c L_c}{D_c A_c}\bar{v} = R\bar{v} \tag{5}$$

where

$$R = \frac{1}{2}\frac{(\mathrm{Re}\, f)\mu P_c L_c}{D_c A_c} \tag{6}$$

R can be considered as the fluidic resistance of the channel. Eq. (5) shows that for a given dimensions straight channel, the pressure drop is proportional to the mean velocity because the fluidic resistance of channel is constant.

2.3. Resistance at corners

The flow resistance at the straight channels is discussed above, and the resistance at the corners will be discussed in this section. As shown in Fig. 2, there are two kinds of corners, T shape and L shape, for a parallel channel. R_i, A_i, P_i are the flow resistance, the cross-sectional area and the cross-sectional perimeter of each straight channel, respectively. R_i can be calculated by Eq. (6) if geometric dimensions are given. The arrangement strategy of the resistance at these places will be discussed below.

2.3.1. T shape

The discrete model for T shape corner is shown in Fig. 2(c), R_{T3} is quite small compared with R_3 because of the long length of channel. Then R_{T3} can be neglected.

R_{T2} can be considered according to the force balance:

$$p_1 A_h - p_2 A_h = \tau_w A_T \tag{7}$$

where A_T represents the contact surface at T shape corner. For a T shape corner, A_T is shown in Fig. 3 with black color.

Hence, R_{T2} is obtained with Eqs. (2)–(4) and (7)

$$R_{T2} = \frac{\mu(\mathrm{Re}\, f)A_T}{2D_c A_h} \tag{8}$$

2.3.2. L shape

The discrete model for L shape corner is shown in Fig. 2(D), R_L is quite small compared with R_2 because of the long length of channel. Then R_L can also be neglected.

After the rearrangement, the resistance at the corners will not be involved into the resistance matrix, because it has been considered in the calculation of straight channels. This rearrangement facilitates the calculation and the availability of the rearrangement will be validated in Section 3.

2.4. Analytical model for parallel channel

Generally speaking, there are two types of parallel-channel configurations, namely Z-type and U-type (Fig. 4). Each type has an inlet header and an outlet header. In a Z-type configuration, the inlet is near the first channel and the outlet is near the last channel. While in a U-type configuration, both the inlet and outlet are near the first channel.

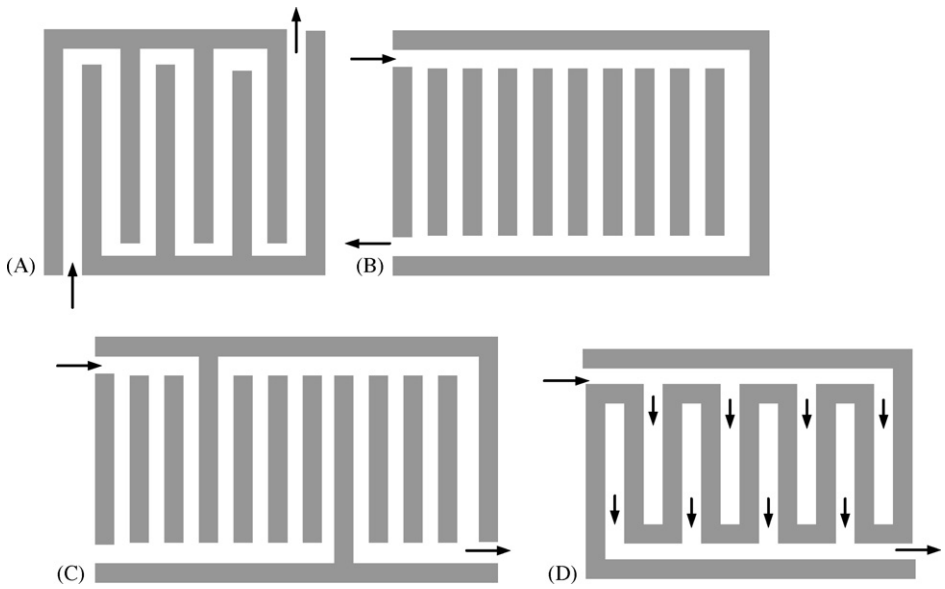

Fig. 1. Schematic diagram of (A) serpentine; (B) parallel; (C) discontinuous; (D) interdigitated type channel configurations.

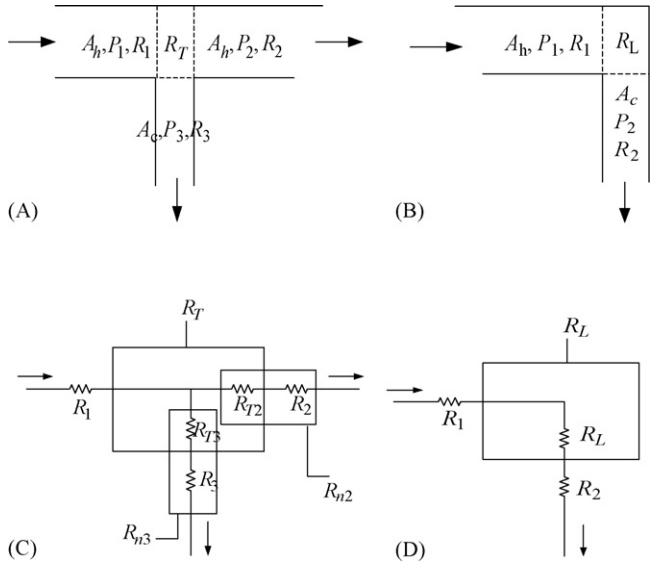

Fig. 2. (A) T shape corner, (B) L shape corner (C) discrete model for T shape corner and (D) discrete model for L shape.

In order to get velocity distribution of a parallel configuration with n channels, a parallel configuration with 3 channels will be discussed first.

2.4.1. Model for a 3-channel plate

2.4.1.1. Z-type configuration. Consider a Z-type parallel configuration with 3 channels shown in Fig. 5A. The flow field is discretized first as shown in Fig. 5B, and the analytical model will be set up

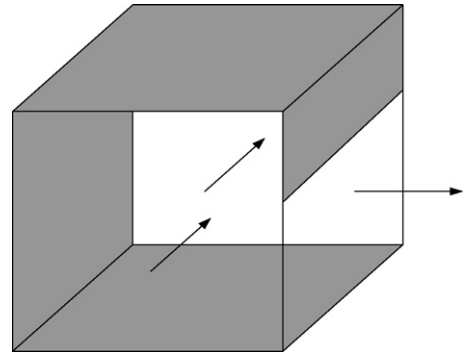

Fig. 3. Schematic diagram of A_T.

based on solving the pressure and mass balance equations. It is assumed that the cross-sectional area of the inlet header, which is represented by A_h, is uniform, and is equal to that of the outlet header, the cross-sectional area of the ith channel represented by A_i is not necessary uniform.

As shown in Fig. 5B, P_i is the pressure at dividing or combing points, V_i is the mean velocity in the inlet header between ith and $i+1$th channel, $V_{i'}$ is the mean velocity in the outlet header between ith and $i+1$th channel, R_i is the resistance of the inlet header between ith and $i+1$th channel, $R_{i'}$ is the resistance of the outlet header between ith and $i+1$th channel, v_i and r_i are the mean velocity and the resistance of the ith channel, respectively.

According to the pressure balance,

$$v_1 r_1 + V_{1'} R_{1'} = V_1 R_1 + v_2 r_2 \quad (9)$$

$$v_2 r_2 + V_{2'} R_{2'} = V_2 R_2 + v_3 r_3 \quad (10)$$

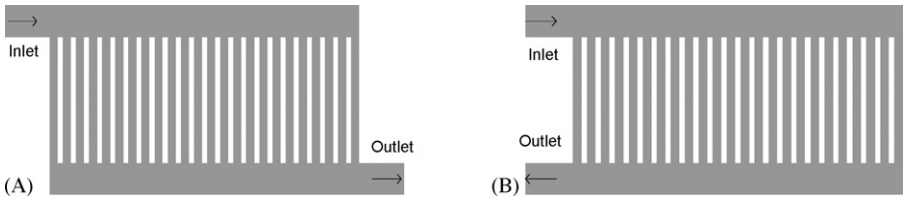

Fig. 4. Schematic diagram of (A) Z-type and (B) U-type parallel-channel flow configurations.

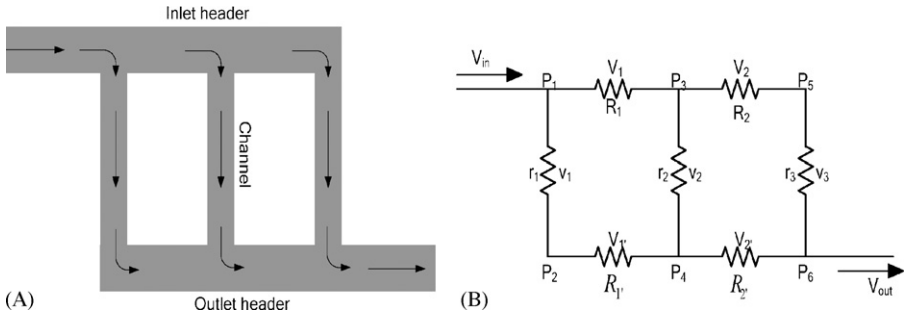

Fig. 5. Schematic diagram of (A) Z-type configuration and (B) discrete channel model.

According to the mass balance,

$$V_{in}A_h = v_1A_1 + V_1A_h \tag{11}$$

$$V_1A_h = V_2A_h + v_2A_2 \tag{12}$$

$$V_2A_h = v_3A_3 \tag{13}$$

$$V_1 + V_{1'} = V_{in} \tag{14}$$

$$V_2 + V_{2'} = V_{in} \tag{15}$$

Combining Eqs. (9)–(15),

$$M_{(3)} = R_{(3)}V_{(3)} \tag{16}$$

where

$$M_{(3)} = \begin{bmatrix} -V_{in}R_{1'} \\ -V_{in}R_{2'} \\ V_{in}A_h \\ 0 \\ 0 \end{bmatrix} \tag{16a}$$

$$R_{(3)} = \begin{bmatrix} r_1 & -r_2 & 0 & -(R_1+R_{1'}) & 0 \\ 0 & r_2 & -r_3 & 0 & -(R_2+R_{2'}) \\ A_1 & 0 & 0 & A_h & 0 \\ 0 & A_2 & 0 & -A_h & A_h \\ 0 & 0 & A_3 & 0 & -A_h \end{bmatrix} \tag{16b}$$

$$V_{(3)} = \begin{bmatrix} v_1 \\ v_2 \\ v_3 \\ V_1 \\ V_2 \end{bmatrix} \tag{16c}$$

2.4.1.2. U-type configuration. Similarly, consider a U-type parallel configuration with 3 channels as shown in Fig. 6.

According to the pressure balance,

$$v_1r_1 = V_1R_1 + v_2r_2 + V_{1'}R_{1'} \tag{17}$$

$$v_2r_2 = V_2R_2 + v_3r_3 + V_{2'}R_{2'} \tag{18}$$

According to the mass balance,

$$V_{in}A_h = v_1A_1 + V_1A_h \tag{19}$$

$$V_1A_h = V_2A_h + v_2A_2 \tag{20}$$

$$V_2A_h = v_3A_3 \tag{21}$$

$$V_1 = V_{1'} \tag{22}$$

$$V_2 = V_{2'} \tag{23}$$

Combining Eqs. (17)–(23),

$$M_{(3)} = R_{(3)}V_{(3)} \tag{24}$$

where

$$M_{(3)} = \begin{bmatrix} 0 \\ 0 \\ V_{in}A_h \\ 0 \\ 0 \end{bmatrix} \tag{24a}$$

$$R_{(3)} = \begin{bmatrix} r_1 & -r_2 & 0 & -(R_1+R_{1'}) & 0 \\ 0 & r_2 & -r_3 & 0 & -(R_2+R_{2'}) \\ A_1 & 0 & 0 & A_h & 0 \\ 0 & A_2 & 0 & -A_h & A_h \\ 0 & 0 & A_3 & 0 & -A_h \end{bmatrix} \tag{24b}$$

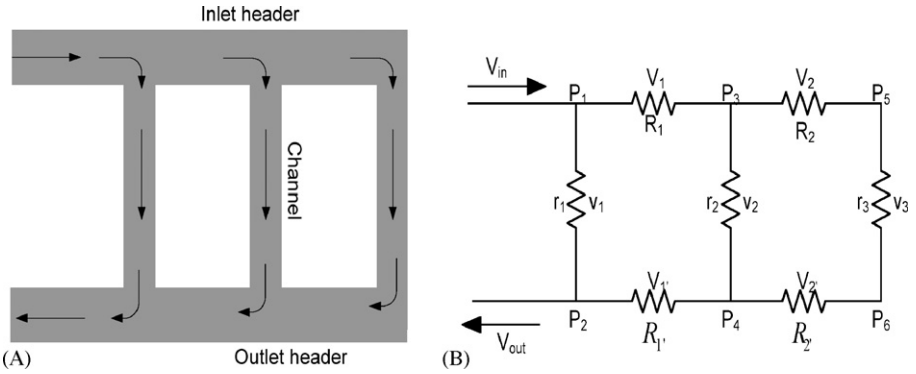

Fig. 6. Schematic diagram of (A) U-type configuration and (B) discrete channel model.

$$V_{(3)} = \begin{bmatrix} v_1 \\ v_2 \\ v_3 \\ V_1 \\ V_2 \end{bmatrix} \tag{24c}$$

Eqs. (16) and (24) inform that, for a parallel configuration with 3 channels, r_i, $R_{i'}$ and R_i is known according to Eqs. (6) and (8). If we know the inlet velocity V_{in}, then, we can solve the matrix equation to get the mean velocity of each channel.

2.4.2. Model for an n-channel plate

Similarly, we now consider a parallel configuration with n channels.

2.4.2.1. Z-type configuration. The schematic diagram of the continuous channel and discrete channel model of Z-type configuration are shown in Fig. 7.

Like the method mentioned in Section 2.4.1, a matrix equation similar to Eq. (16) will be set up.

$$M_{(n)} = R_{(n)} V_{(n)} \tag{25}$$

$$M_{(n)} = \begin{bmatrix} -V_{\text{in}} R_{1'} \\ -V_{\text{in}} R_{2'} \\ \vdots \\ -V_{\text{in}} R_{(n-1)'} \\ V_{\text{in}} A_{\text{h}} \\ \left.\begin{matrix} 0 \\ 0 \\ \vdots \\ 0 \end{matrix}\right\} n-1 \end{bmatrix} \tag{25a}$$

where

$$R_{(n)} = \begin{bmatrix} \left.\begin{matrix} r_1 & -r_2 & 0 & 0 & 0 \cdots 0 & -(R_1+R_{1'}) & 0 & 0 & 0 \cdots 0 \\ 0 & r_2 & -r_3 & 0 & 0 \cdots 0 & 0 & -(R_2+R_{2'}) & 0 & 0 \cdots 0 \\ 0 & 0 & r_3 & -r_4 & 0 \cdots 0 & 0 & 0 & -(R_3+R_{3'}) & 0 \cdots 0 \\ \vdots & \vdots & & \ddots & \ddots & \vdots & & & \ddots \\ 0 & 0 & \cdots & \cdots & 0\ r_{n-1} & -r_n & 0 & 0 \cdots & 0 -(R_{n-1}+R_{(n-1)'}) \end{matrix}\right\} n-1 \\ \left.\begin{matrix} A_1 & 0 & 0 & 0 & 0 \cdots 0 & A_h & 0 & 0 & 0 \cdots 0 \\ 0 & A_2 & 0 & 0 & 0 \cdots 0 & -A_h & A_h & 0 & 0 \cdots 0 \\ 0 & 0 & A_3 & 0 & 0 \cdots 0 & 0 & 0 & -A_h & A_h \cdots 0 \\ \vdots & \vdots & & \ddots & \ddots & \vdots & & & \ddots \\ 0 & 0 & \cdots & \cdots & A_{n-1}\ 0 & 0 & 0 & 0 \cdots & -A_h\ A_h \\ 0 & 0 & \cdots & \cdots & 0\ A_n & 0 & 0 & 0 \cdots & 0 -A_h \end{matrix}\right\} n \\ \underbrace{\qquad\qquad}_{n} \quad \underbrace{\qquad\qquad\qquad}_{n-1} \end{bmatrix} \tag{25b}$$

$$V_{(n)} = \begin{bmatrix} v_1 \\ v_2 \\ \vdots \\ v_n \\ V_1 \\ V_2 \\ \vdots \\ V_{n-1} \end{bmatrix} \tag{25c}$$

The dimension of resistance matrix R is expanded from 5×5 to $(2n-1) \times (2n-1)$.

2.4.2.2. U-type configuration. The schematic diagram of the continuous channel and discrete channel model of U-type configuration are shown in Fig. 8.

A matrix equation for U-type is set up by the method mentioned above.

$$M_{(n)} = R_{(n)} V_{(n)} \tag{26}$$

where

$$M_{(n)} = \begin{bmatrix} \left.\begin{matrix} 0 \\ 0 \\ \vdots \\ 0 \end{matrix}\right\} n-1 \\ V_{\text{in}} A_{\text{h}} \\ \left.\begin{matrix} 0 \\ 0 \\ \vdots \\ 0 \end{matrix}\right\} n-1 \end{bmatrix} \tag{26a}$$

$$R_{(n)} = \begin{bmatrix} \left.\begin{matrix} r_1 & -r_2 & 0 & 0 & 0 \cdots 0 & -(R_1+R_{1'}) & 0 & 0 & 0 \cdots 0 \\ 0 & r_2 & -r_3 & 0 & 0 \cdots 0 & 0 & -(R_2+R_{2'}) & 0 & 0 \cdots 0 \\ 0 & 0 & r_3 & -r_4 & 0 \cdots 0 & 0 & 0 & -(R_3+R_{3'}) & 0 \cdots 0 \\ \vdots & \vdots & & \ddots & \ddots & \vdots & & & \ddots \\ 0 & 0 & \cdots & \cdots & 0\ r_{n-1} & -r_n & 0 & 0 \cdots & 0 -(R_{n-1}+R_{(n-1)'}) \end{matrix}\right\} n-1 \\ \left.\begin{matrix} A_1 & 0 & 0 & 0 & 0 \cdots 0 & A_h & 0 & 0 & 0 \cdots 0 \\ 0 & A_2 & 0 & 0 & 0 \cdots 0 & -A_h & A_h & 0 & 0 \cdots 0 \\ 0 & 0 & A_3 & 0 & 0 \cdots 0 & 0 & 0 & -A_h & A_h \cdots 0 \\ \vdots & \vdots & & \ddots & \ddots & \vdots & & & \ddots \\ 0 & 0 & \cdots & \cdots & A_{n-1}\ 0 & 0 & 0 & 0 \cdots & -A_h\ A_h \\ 0 & 0 & \cdots & \cdots & 0\ A_n & 0 & 0 & 0 \cdots & 0 -A_h \end{matrix}\right\} n \\ \underbrace{\qquad\qquad}_{n} \quad \underbrace{\qquad\qquad\qquad}_{n-1} \end{bmatrix} \tag{26b}$$

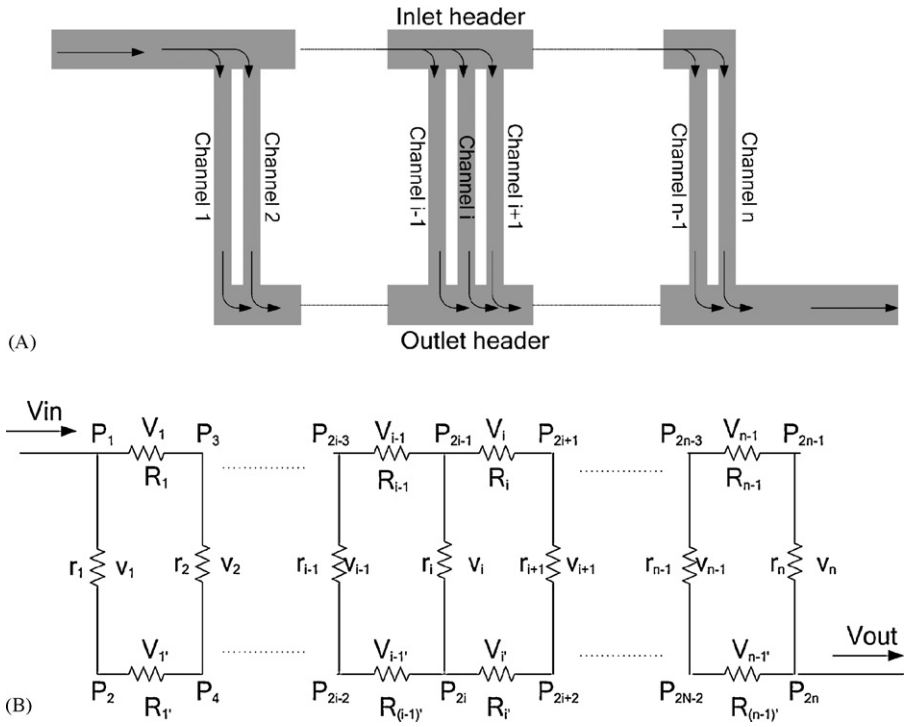

Fig. 7. Schematic diagram of (A) Z-type configuration and (B) discrete channel model.

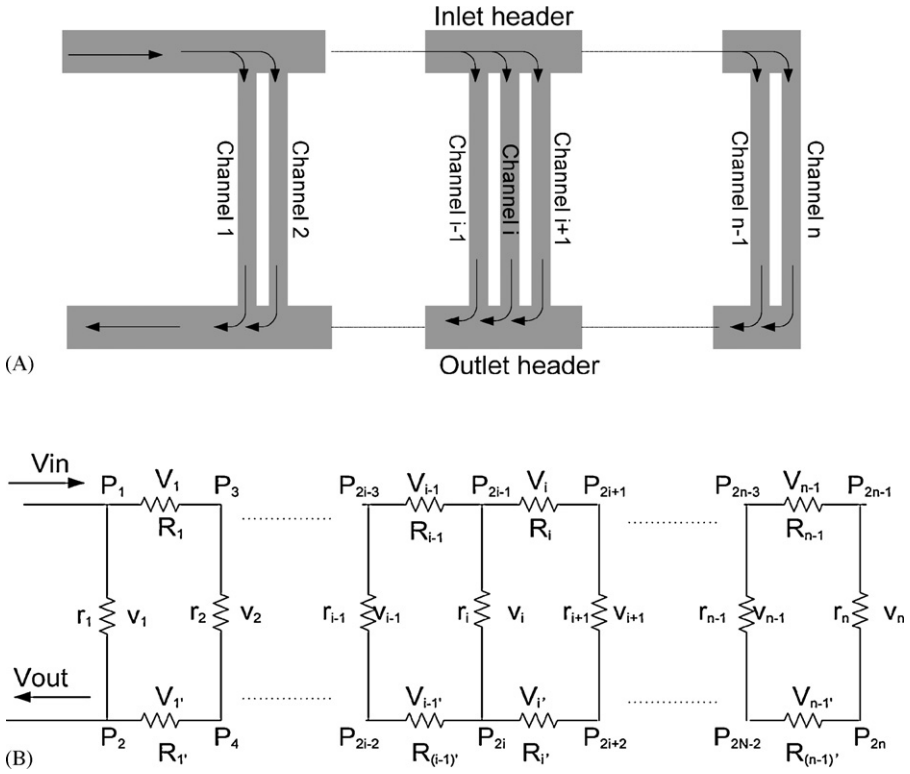

Fig. 8. Schematic diagram of (A) U-type configuration and (B) discrete channel model.

$$V_{(n)} = \begin{bmatrix} v_1 \\ v_2 \\ \vdots \\ v_n \\ V_1 \\ V_2 \\ \vdots \\ V_{n-1} \end{bmatrix} \quad (26c)$$

The dimension of resistance matrix R is also expanded from 5×5 to $(2n-1) \times (2n-1)$.

As shown in Eqs. (25) and (26), there are $2n-1$ unknown variables and $2n-1$ equations. So we can solve the matrix equations to get the velocity of each channel.

3. Validation

The accuracy of the presented model is verified by comparing the result of the discrete model with that of the three-dimensional CFD simulations.

Here, the flow distribution of parallel channel configurations are simulated using the commercial CFD code CFD-ACE+ developed by CFD Research Corporation.

First, we study the flow distribution of 11-channel plates. Then, the number of channels is extended to 21 to examine the accuracy of the analytical model with more channels. The geometrical dimensions of the plate are shown in Fig. 9.

As shown in Fig. 9, channels and ribs are distributed uniformly with a width of 1.5 mm, and the width of the inlet header and outlet header are 3 mm, both of the depth of the channels and headers are 0.6 mm.

A comparison of the velocity distribution obtained form the discrete model and CFD simulation is shown in Fig. 10. There is an acceptable agreement between the analytical and CFD results.

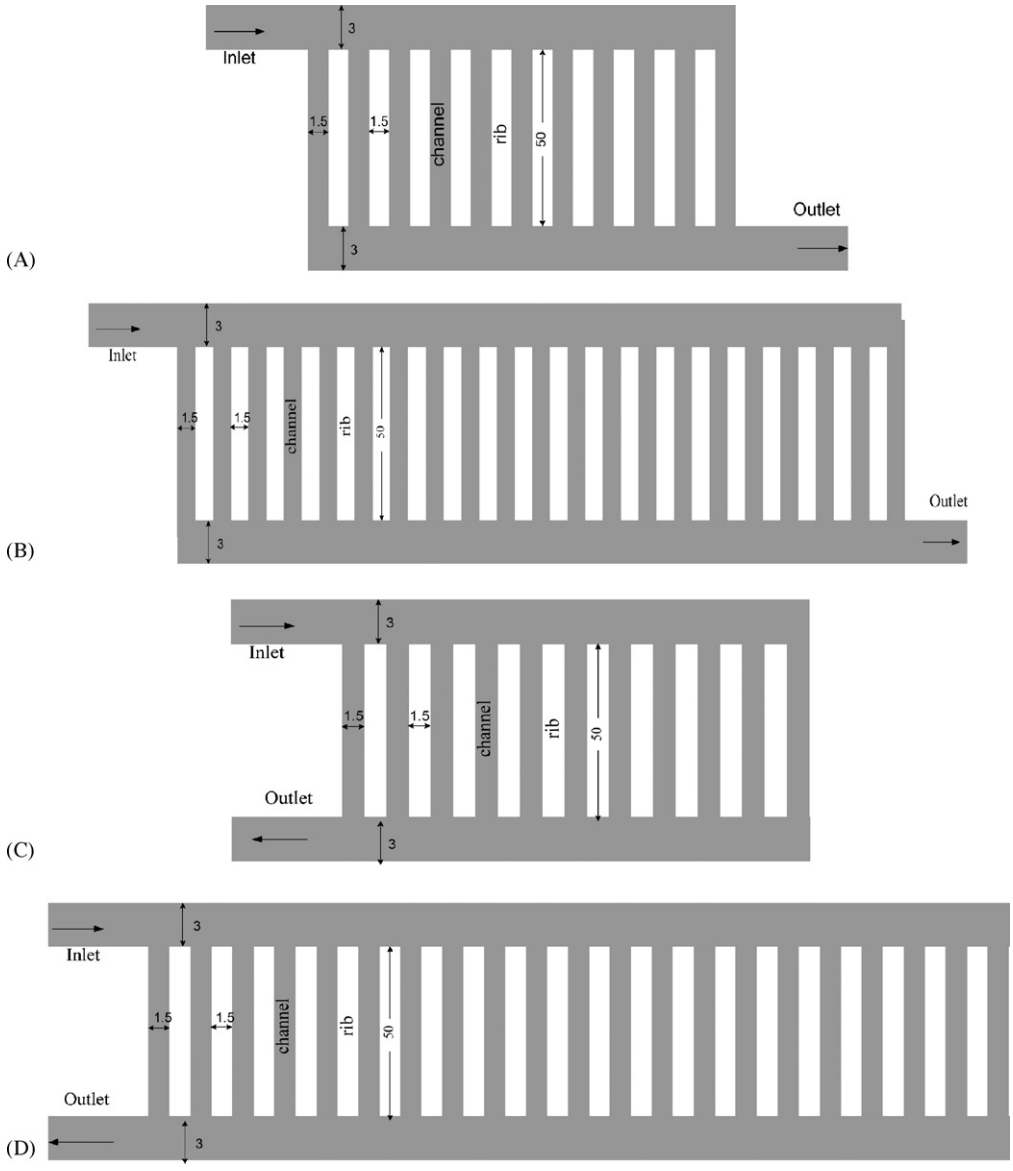

Fig. 9. Schematic diagrams of (A) Z-type 11-channel (B) Z-type 21-channel (C) U-type 11-channel and (D) U-type 21-channel plate (units: mm).

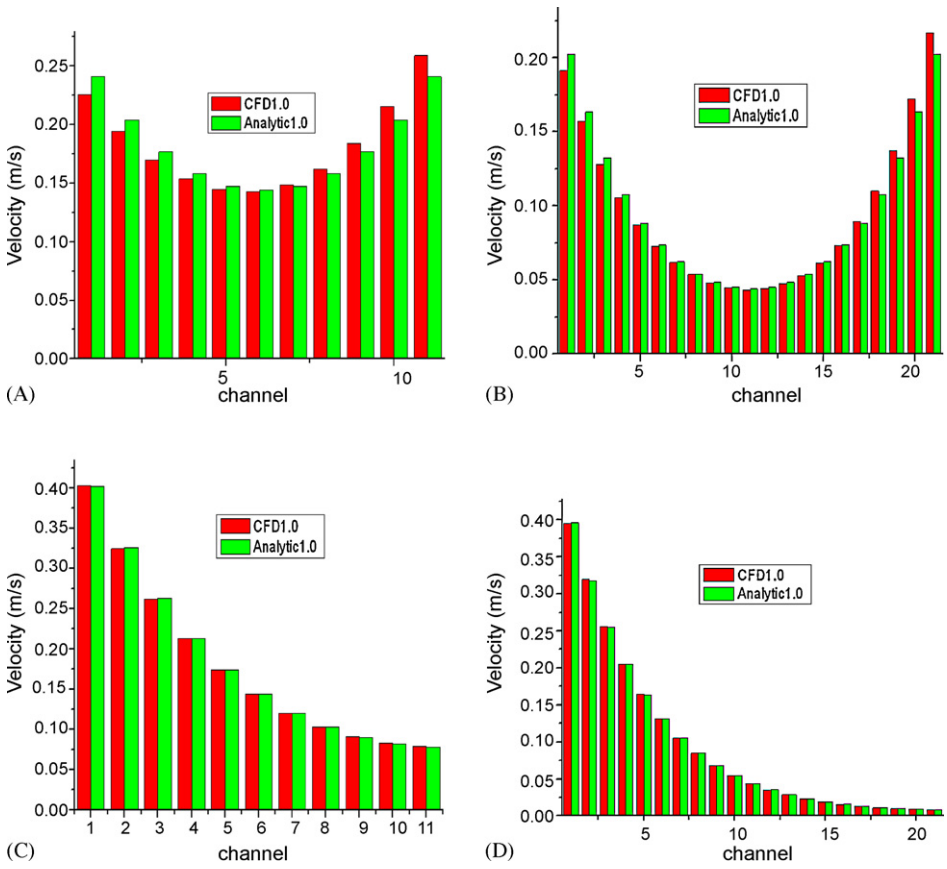

Fig. 10. Comparison of the results from CFD and analytical model (A) Z-type 11-channel (B) Z-type 21-channel (C) U-type 11-channel and (D) U-type 21-channel plate.

4. Optimization

As mentioned above, parallel channels have low pressure drop but they also cause flow maldistribution which can also be observed from Fig. 10. It is possible to have a uniform flow distribution in the parallel channels by having a very large header cross-sectional area compared with that of the channel. Unfortunately, this will decrease the active geometrical area of the bipolar plate. A uniform flow distribution in the parallel channels can also be obtained by changing the cross-sectional area of the channels, increasing the cross-sectional area of the central channels which has low velocities, decreasing the cross-sectional area of the channels near the inlet and outlet which has high velocities.

According to the model proposed in section 3, high-performance language MATLAB program is developed to optimize the flow distribution of an 11-channel Z-type plate. The original geometric parameters of the plate have been shown in Fig. 9(A) and the variables, object function and constraints will be discussed below.

4.1. Variables

The geometric dimensions of the plate are treated as constants except the width of each channel $l(i)$ and the length of the header between each channel $L(i)$ (Fig. 11). For an 11-channel plate, there are 21 variables: $l(1)$, $l(2)$, . . ., $l(11)$ and $L(1)$, $L(2)$, . . ., $L(10)$.

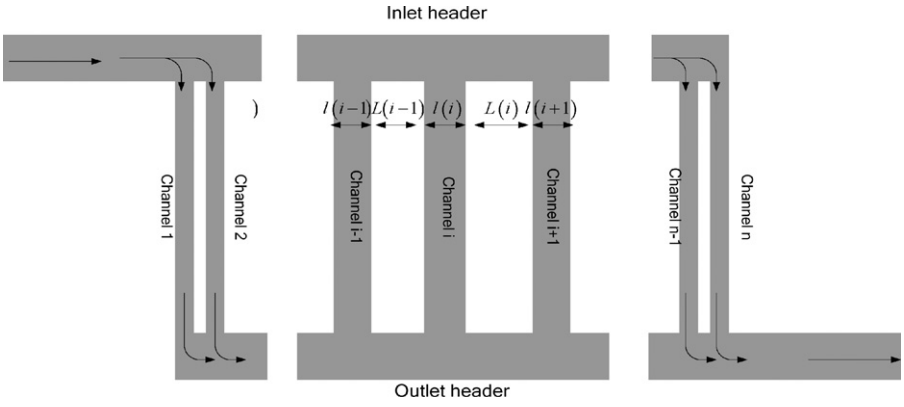

Fig. 11. Variables of the bipolar plates.

Table 1
Widths of the channels (units: mm).

$l(1)$	$l(2)$	$l(3)$	$l(4)$	$l(5)$	$l(6)$	$l(7)$	$l(8)$	$l(9)$	$l(10)$	$l(11)$
0.8	0.8750	0.9514	1.0237	1.0779	1.0983	1.0779	1.0237	0.9514	0.8750	0.8

4.2. Objective function

Non-uniformity index, F, is defined as follows [6,7]:

$$F = \frac{\sqrt{\sum_{i=1}^{n}(v_i - \bar{v})^2}}{n\bar{v}} \tag{27}$$

characterizing the relative flow split is treated as object function. Where v_i is a function of $l(i)$ and $L(i)$

$$v_i = f(l(i), L(i)) \tag{28}$$

For an 11-channel plate, F can be expressed as:

$$F = \frac{\sqrt{\sum_{i=1}^{11}(v_i - \bar{v})^2}}{11\bar{v}} \tag{29}$$

Here, F represents the non-uniformity of the flow distribution. If F equals to zero, all channels have the same flow velocity. The goal of this section is to minimize F by changing the variables $l(i)$ and $L(i)$.

4.3. Constraints

As mentioned above, in order to obtain a uniformly distributed flow field, we should increase the cross-sectional area of the channels in the center of the plate, and decrease the cross-sectional area of the channels near the inlet and outlet. For engineering purpose, bipolar plates should be symmetric, and we hope the width of channels and ribs are in the range of 0.8–1.5 mm. So, the constraints

Table 2
Lengths of the headers (units: mm).

$L(1)$	$L(2)$	$L(3)$	$L(4)$	$L(5)$	$L(6)$	$L(7)$	$L(8)$	$L(9)$	$L(10)$	$L(11)$
0.8	0.8	0.8	0.8	0.8	0.8	0.8	0.8	0.8	0.8	0.8

are:

$$\begin{gathered} l(1) = l(11), l(2) = l(10), \ldots l(5) = l(7) \\ L(1) = L(10), L(2) = L(9), \ldots L(5) = L(6) \\ l(1) > l(2) > l(3) > l(4) > l(5) > l(6) \\ 0.8 < l(i),\ \ L(i) < 1.5 \end{gathered} \tag{30}$$

4.4. Results

The commercial software MATLAB is used to optimize the flow field, and the optimized results are listed in Tables 1–3.

Table 1 shows the widths of the channels. After optimization, the smallest channel has a width of 0.8 mm, and the largest channel has a width of 1.0983 mm. Table 2 shows the length of the header between channels. Table 3 shows the mean velocities of the channels from analytical model, which indicates that the velocities at different channels are nearly equal and a uniformly distributed flow field is obtained according to analytical results.

The objective parameter F for the plate before optimization and after optimization is 0.0580 and 0.0065, respectively. Flow distribution of the optimized plate becomes more uniform than the original design. Fig. 12 shows the magnitude of the velocity comparison of the contours results obtained from CFD simulation before and after optimization.

Table 3
Mean velocities of the channels from analytical model (units: m s^{-1}).

$v(1)$	$v(2)$	$v(3)$	$v(4)$	$v(5)$	$v(6)$	$v(7)$	$v(8)$	$v(9)$	$v(10)$	$v(11)$
0.2834	0.2836	0.284	0.2842	0.2842	0.2842	0.2842	0.2842	0.2844	0.2848	0.2852

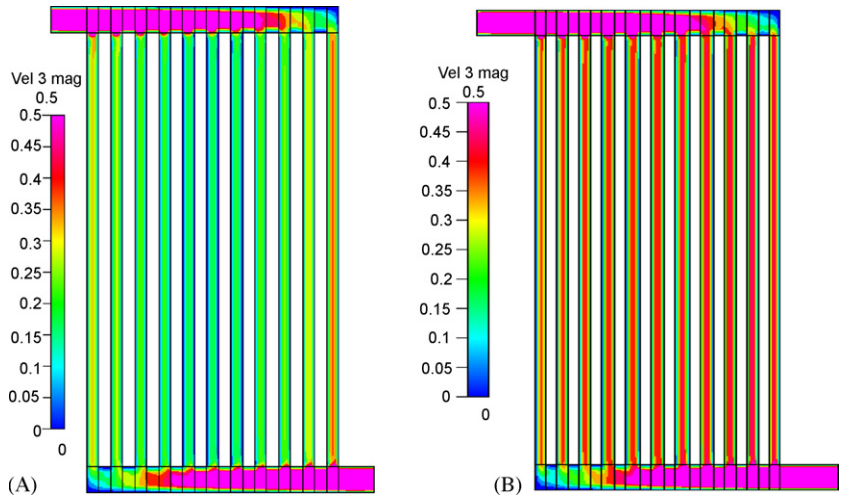

Fig. 12. Comparison of the contour results from CFD simulation (units: m s^{-1}). (A) Before optimization and (B) after optimization.

5. Conclusions

The flow distribution is one of the important determinants of fuel-cell efficiency. Unfortunately, parallel-channel plates often suffer from severe flow maldistribution. In the present study, a high efficacy analytical model, in the form of matrix equation, is presented to calculate the flow distribution of the parallel channels of Z-type configurations and U-type configurations, respectively.

Furthermore, the model is validated by comparison with the results obtained from CFD simulations and it has good agreement with CFD results.

According to the simulation results, it is found that a uniform flow distribution in the parallel channels can also be obtained by changing the cross-sectional area of the channels. Therefore, the analytical model is used to optimize the geometric dimensions of the plate, and a more uniformly distributed flow field is obtained. It could be very helpful in the concept design of flow channel for bipolar plates.

Acknowledgements

This work is supported by National Natural Science Foundation of China (No.50805092), Major International (Regional) Joint Research Project of NSFC (No. 50820125506) and China Postdoctoral Science Foundation (No. 20080430665). The authors would like acknowledge their financial support.

References

[1] Xianguo Li, Imran Sabir, Int. J. Hydrogen Energy 30 (2005) 359–371.
[2] H.-M. Jung, W.-Y. Lee, J.-S. Park, C.-S. Kim, Int. J. Hydrogen Energy 29 (2004) 945–954.
[3] S. Maharudrayya, S. Jayanti, A.P. Deshpande, J. Power Sources 157 (2006) 358–367.
[4] Z. Ma, S.M. Jeter, S.I. Abdel-Khalik, Int. J. Hydrogen Energy 28 (2003) 85–97.
[5] P. Pei, M. Ouyang, W. Feng, L. Lu, H. Huang, J. Zhang, Int. J. Hydrogen Energy 31 (2006) 371–377.
[6] R.J. Kee, P. Korada, K. Walters, M. Pavol, J. Power Sources 109 (2002) 148–159.
[7] S. Maharudrayya, S. Jayanti, A.P. Deshpande, J. Power Sources 144 (2005) 94–106.
[8] H.M. Jung, W.Y. Lee, J.S. Park, C. Kim, Int. J. Hydrogen Energy 29 (2004) 945–954.
[9] S. Shimpalee, J.W. Van Zee, Int. J. Hydrogen Energy 32 (2007) 842–856.
[10] H.J. Koh, K.H. Seo, G.C. Lee, S.Y. Yoo, C.H. Lim, Pressure and flow distribution in internal gas manifolds of a fuel-cell stack, J. Power Sources 115 (2003) 54–65.
[11] Z. Ma, S.M. Jeter, S.I. Abdel-Khalik, Flow network analysis application in fuel cells, J. Power Sources 108 (2002) 106–112.
[12] G. Karimi, J.J. Baschuk, X. Li, Performance analysis and optimization of PEM fuel cell stacks using flow network approach, J. Power Sources 147 (2005) 162–177.
[13] D. Martin, D.M. Guinea, B. Moreno, L. Gonzalez, M.C. Garcia-Alegre, D. Guinea, Electric modelling and image analysis of channel flow in bipolar plates, Int. J. Hydrogen Energy 32 (2007) 1572–1581.
[14] W.M. Kays, M.E. Crawford, Convective Heat and Mass Transfer, McGraw-Hill, New York, 1980.